A Monolithically Integrated ACP-OPLL Receiver for RF/Photonic Links

Yifei Li, Ashish Bhardwaj, Renyuan Wang, Sheilei Jin, Larry A. Coldren, *Fellow, IEEE*, John E. Bowers, *Fellow, IEEE*, and Peter Herczfeld, *Fellow, IEEE*

Abstract—The first monolithically integrated optical phase-locked loop (OPLL) employing attenuating-counter-propagating waves is presented. It demonstrates the highest dynamic range among monolithically integrated OPLLs. Its performance is limited by the bandwidth and linearity of the photodetectors used in the OPLL.

Index Terms—Dynamic range, optical phase-locked loop (OPLL), phase demodulation, photonic integrated circuit.

I. INTRODUCTION

IT is desirable to replace bulky coaxial cables by fiber-optic links in advanced radar systems. However, the adaptation of fiber-optic links is still limited by their small Spurious Free Dynamic Range (SFDR). Many critical radar applications (such as channelized EW receivers) require an SFDR larger than 140 dB· $Hz^{2/3}$, which is orders of magnitude higher than what is available with current state of the art. As a solution, a new phase modulated (PM) fiber-optic link employing an Optical Phase-Locked-Loop (OPLL) linear phase demodulator has been proposed [1], [2]. The OPLL demodulates the optical phase by tight phase tracking. It requires a large open loop gain over a wide bandwidth. Thus, its feedback stability only tolerates a very short loop delay (< 10 ps). To realize such a short delay requirement, a novel Attenuation Counter-Propagating (ACP) OPLL has been proposed [2]. The ACP approach eliminates the phase delays arising from the phase modulators and the photodetectors within the OPLL. The ACP-concept has been validated in a hybrid integrated OPLL that consists of an ACP LiNbO₃ local phase modulator and a pair of bulk photodetectors [2]. In this letter, we present the first monolithically integrated ACP-OPLL Photonic Integrated Circuit (PIC) on an

Y. Li, R. Wang, and S. Jin are with the Department of Electrical and Computer Engineering, University of Mass, Dartmouth, MA 02747 USA (e-mail: yli2@umassd.edu).

A. Bhardwaj, L. A. Coldren, and J. E. Bowers are with the Department of Electrical and Computer Engineering, the University of California Santa Barbara, CA 93106, USA (e-mail: ashishb@ece.ucsb.edu).

P. Herczfeld is with the Department of Electrical and Computer Engineering, Drexel University, Philadelphia, PA 19104, USA (e-mail: herczfeld@ece.drexel.edu).
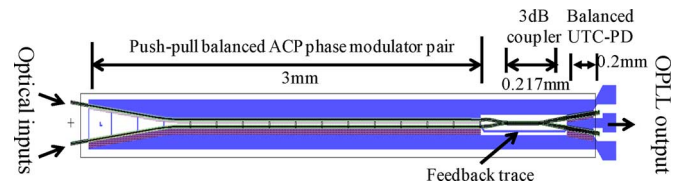
Fig. 1. ACP-OPLL photonic integrated circuit.

Indium Phosphide (InP)-based material platform. Details regarding its fabrication are reported in [3].

II. ACP-OPLL PHOTONIC INTEGRATED CIRCUIT

A mask layout of the ACP-OPLL PIC is shown in Fig. 1. It consists of a pair of push-pull ACP optical phase modulators, a pair of balanced uni-traveling carrier (UTC) waveguide photodetectors, a 3-dB optical coupler and a feedback trace that connects the balanced photodetectors to the phase modulators. Similar to previous OPLL PICs [1], the ACP-OPLL loop components share a multi-quantum well (MQW) optical waveguide to facilitate photonic integration. The MQW region contains 25 periods of lattice-matched $In_{0.65}Ga_{0.35}As_{0.76}P_{0.24}$ wells (9 nm thick) and $In_{0.8}Ga_{0.2}As_{0.44}P_{0.56}$ barriers (6.5 nm thick). Stand-alone phase modulators using this quantum well design showed excellent linear phase modulation range (ϕ_{IP3}) per unit length ($\sim 4\pi$/mm) and low optical loss (< 1 dB/mm) [4].

To improve lateral confinement, the phase modulators inside the ACP-OPLL PIC are realized as deep ridge optical waveguides with a width of 2.5 μm. The push-pull modulator pair is 3 mm long providing a combined ϕ_{IP3} of 24π, which is sufficient to enable an OPLL with an SFDR ~ 140 dB · $Hz^{2/3}$. To eliminate the latency, the phase modulator pair uses counter-propagating optical and RF modulation fields, where the RF modulation field is attenuated by the n- and the p-lossy electrodes of the push-pull modulator pair (see Fig. 2). Both lossy electrodes have a series resistance of ~ 150 Ω. Fig. 3 shows the simulated response of the phase modulator pair. The simulated phase modulation sensitivity is 2.5 rad/volt, which corresponds to a V_π of 1.26 V. Its 3-dB bandwidth is 1.15 GHz. The phase response of the ACP phase modulator pair is bound between 0 and $\pi/2$, suggesting a lumped-element response that is free of propagation delay.

The layers that define the UTC-waveguide photodetector were developed by Klamkin *et al.* [5], and are grown on top of the phase modulator MWQs in the base-epitaxial wafer used in the fabrication of the ACP-OPLL PIC. This UTC-waveguide photodetector design can generate a large photocurrent (> 50 mA) with high photodetection linearity
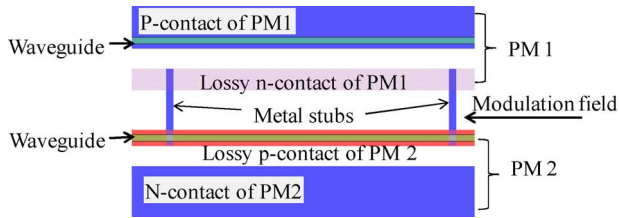
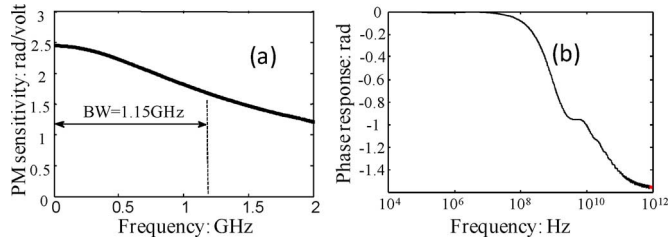Fig. 2. A section of push-pull ACP phase modulator.

Fig. 3. Phase modulator response. (a) Magnitude response. (b) Phase response.

TABLE I
LOOP COMPONENT MEASUREMENTS

Component		Measurement	Design goal
Push-pull phase modulator pair	Optical loss	~2dB/mm	<1dBm/mm
	V_π	~1.2 V	~1.26 V
3-dB coupler	Insertion loss	~1 dB	<1 dB
	Splitting ratio	50.7:49.3	50:50
Single waveguide UTC-PD	Bandwidth *	<200 MHz	2.76 GHz
	Quantum eff.*	<50%	100%
	OIP3*	~13 dBm	>40 dBm

*The PD measurements were taken with 5 mA photocurrent, 6 V reverse bias, and a 50-Ω termination. The performance improves at a higher bias voltage but deteriorates with a larger photocurrent (or higher input power).

(OIP3 > 40 dBm) [5]. To eliminate its latency, the photodetector also employs the counter-propagating optical and RF fields. The width and the length of the photodetector are 10 μm and 200 μm, respectively. Based on the dimensions, a single photodetector should exhibit an *RC* time limited bandwidth of 2.76 GHz.

The photodetectors and the phase modulators are connected by a Multi-Mode Interference (MMI) 3-dB coupler to form the ACP-OPLL PIC. The coupler is 7 μm wide and 217 μm long. The complete loop delay of the ACP-OPLL, which is determined by the coupler and the feedback path, is $\sim$ 10 ps.

III. EXPERIMENTAL RESULTS

The loop components of the ACP-OPLL PIC were first characterized using discrete components that were co-fabricated with the ACP-OPLL PIC on the same epitaxial wafer. The measurement results are summarized in Table I. The 3-dB coupler showed low insertion loss and ideal splitting ratio. The modulator pair also showed good V_π. However, the photodetector showed narrow bandwidth, small responsivity, and poor linearity (OIP3) compared to the design goals that were based on the photodetectors in [5].

Next, the ACP-OPLL receiver was characterized within a phase modulated optical link (see Fig. 4). The output of a fiber
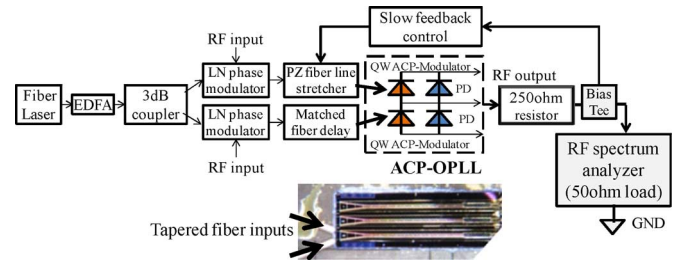

Fig. 4. PM link experimental setup.

laser operating at 1.55 μm was amplified using an erbium doped fiber amplifier (EDFA) unit, and then split into two paths using a polarization maintaining 3-dB optical coupler. Each path contains a transmitter (Tx) LiNbO$_3$ optical phase modulator with V_π of 4.5 V. The RF inputs are applied to the LiNbO$_3$ phase modulators. Phase modulated optical signals are launched into the waveguide inputs of the ACP-OPLL using a tapered fiber with a 2.5 μm spot diameter. The coupling loss between the tapered fiber and the optical waveguide was measured to be $\sim$ 2.5 dB. To ensure a sufficient open loop gain in presence of poor photodetector responsivity, a 300 Ω load impedance was used at the ACP-OPLL output. Ideally, this should be accomplished using an impedance transformer. However, a simpler approach was taken by inserting a 250 Ω series resistor between the output of the ACP-OPLL and the external 50 Ω load. Due to this arrangement, the power captured at the RF spectrum analyzer is 7.78 dB lower than the RF power at the ACP-OPLL output. To overcome environmental perturbations, the slow varying portion of the ACP-OPLL's output was extracted through the DC port of an RF bias-Tee and fed back to a piezo-electric fiber-optic line stretcher to correct for phase errors. This ensures long-term stable phase locking.

The feedback stability of the ACP-OPLL PIC was verified while gradually increasing the optical input power. To avoid facet damage, the optical power launched from each tapered fiber was limited to 200 mW. During this process, no oscillation or other forms of instabilities were observed.

The linearity of the ACP-OPLL PIC was determined using a two-tone inter-modulation test. The optical power launched into each input waveguide was 200 mW. The reverse bias voltage was initially set at 6 V, where the MQW ACP-phase modulators showed good linearity [4]. Each photodetector generated a photocurrent of 12 mA. The ACP-OPLL PIC showed good phase demodulation linearity below 170 MHz. A sample of the 150 MHz output captured at the 50 Ω load is shown in Fig. 5(a). With 7 dBm RF input, the measured inter-modulation distortion (IMD) level was -71 dBc. The link input third order inter-modulation intercept point (IIP3) was measured to be 42.5 dBm (see Fig. 5(b)). Since the LiNbO$_3$ phase modulator at the link input has a V_π of 4.5 V, the IIP3 corresponds to a demodulation ϕ_{IP3} (i.e., the maximum linear phase demodulation range) [4] of 6.9π. In addition, the third order intercept point at the output of the ACP-OPLL (OIP3) is $\sim$ 23.68 dBm. At 150 MHz, the noise power delivered to the 50 Ω external load was measured to be ~ -171 dBm/Hz, from which the ACP-OPLL output noise floor was determined to be ~ -163 dBm/Hz. Thus, the SFDR is $\sim$ 124.5 dB $\cdot$ Hz$^{2/3}$ at 150 MHz.
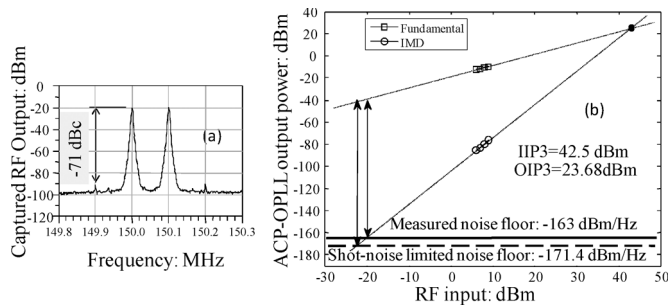
Fig. 5. Distortion measurements at 150 MHz. (a). Captured RF spectrum with 7 dBm RF input. (b) The third order intercept point measurement. The ACP-OPLL output is 7.78 dB higher than the spectrum analyzer reading.
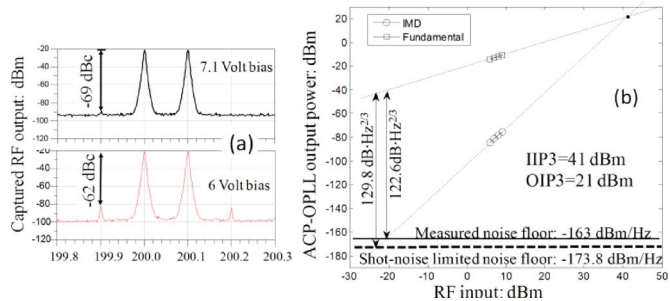
Fig. 6. Distortion measurements at 200 MHz. (a). Captured RF spectrum with 7 dBm RF input. (b) The third order intercept point measurement at 7.1 V bias. The ACP-OPLL output is 7.78 dB higher than the spectrum analyzer reading.
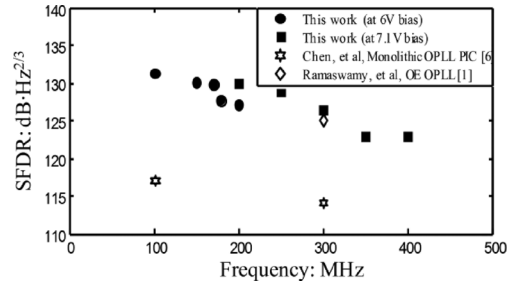
Fig. 7. SFDR in the photodetector shot-noise limit versus RF frequency.

reverse bias voltage further did not enhance the performance of the ACP-OPLL receiver.

The SFDR (in the shot-noise limit) of the ACP-OPLL PIC as a function of RF frequency is summarized in Fig. 7, and the results are compared with the best reported SFDRs (also in the shot-noise limit) of other OPLL PIC devices. Despite the non-ideal photodetectors, the SFDR of the ACP-OPLL PIC is 10 dB higher compared to that observed in earlier monolithically integrated OPLL PICs [6]. At 300 MHz, its SFDR is comparable ($\sim$ 1 dB better) to an optoelectronic (OE) OPLL [1] that requires an external electronic amplifier.

IV. CONCLUSION

The design and characterization of the first monolithically integrated ACP-OPLL PIC have been presented. This device demonstrates the highest SFDR (in shot-noise limit) among monolithically integrated OPLL PICs. Its performance is limited by the bandwidth and the linearity of the photodetectors.

Since this letter is focused on the ACP-OPLL receiver, we also determined the SFDR in the photodetector shot–noise limit. This represents the performance of the ACP-OPLL receiver when the noise from the link transmitter is negligible. The link output noise floor in the shot-noise limit is given by:

$$N_\text{out\_shot\_noise\_limit} = G_{link} \cdot \left(\frac{e}{I_{PD}} \right) \cdot \frac{\left(\frac{V_\pi}{\pi} \right)^2}{Z_{term}} \quad (1)$$

where G_{link} is the link gain, I_{PD} is the photocurrent generated in each photodetector, V_π and Z_{term} are the half wave voltage and the termination resistance of the Tx LiNbO$_3$ phase modulator, respectively. G_{link} was measured to be -18.82 dB. With 12 mA of photocurrent, the output noise floor in the shot-noise limit was calculated to be -171.4 dBm/Hz. Thus, the SFDR in the shot-noise limit is 130.1 dB $\cdot$ Hz$^{2/3}$ at 150 MHz.

The performance of the ACP-OPLL PIC degraded significantly beyond 170 MHz at a reverse bias of 6 V due to the narrow bandwidth observed in the photodetectors. But a higher reverse bias voltage helped to extend the operating bandwidth of the ACP-OPLL PIC. As shown in Fig. 6(a), when the reverse bias voltage was increased to 7.1 V, the distortion level at 200 MHz improved by 7 dB. The IIP3 and OIP3 in this case were 41 dBm and 21 dBm, respectively (see Fig. 6(b)). The measured SFDR was 122.6 dB $\cdot$ Hz$^{2/3}$. The link gain was -20 dB. With a higher reverse bias voltage the photocurrent also increased to 15 mA. The shot-noise limited output noise floor was -173.8 dBm/Hz. Thus, at 200 MHz, the SFDR in the photodetector shot-noise limit was 129.8 dB $\cdot$ Hz$^{2/3}$. Increasing the

REFERENCES

[1] J. Klamkin, L. A. Johansson, A. Ramaswamy, N. Nunoya, S. Ristic, U. Krishnamachari, J. Chen, J. E. Bowers, S. P. DenBaars, and L. A. Coldren, "Highly linear integrated coherent receivers for microwave photonic links," in *Proc. OFC/NFOEC*, San Diego, CA, Mar. 22–26, 2009, OMK4.

[2] Y. Li and P. Herczfeld, "Coherent PM optical link employing ACP-PPLL," *J. Lightw. Technol.*, vol. 27, no. 9, pp. 1086–1094, May 2009.

[3] A. Bhardwaj, Y. Li, R. Wang, S. Jin, P. Herczfeld, J. E. Bowers, and L. A. Coldren, "Monolithic integration of an attenuated counter-propagating optical phase-locked loop coherent receiver," *Electron. Lett.*, submitted for publication.

[4] Y. Li, R. Wang, A. Bhardwaj, S. Ristic, and J. Bowers, "High linearity InP based phase modulators using a shallow quantum well design," *IEEE Photon. Technol. Lett.*, vol. 22, no. 18, pp. 1340–1342, Sep. 2010.

[5] J. Klamkin *et al.*, "Output saturation and linearity of waveguide uni-traveling-carrier photodiodes," *IEEE J. Quantum Electron.*, vol. 44, no. 4, pp. 354–359, Apr. 2008.

[6] C. H. Chen, A. Ramaswamy, J. Klamkin, L. A. Johansson, J. E. Bowers, and L. A. Coldren, "Optical phase demodulation using a coherent receiver with an ultra-compact grating beam splitter," in *Proc. Asia Opt. Fiber Commun. Optoelectron. Expo. Conf.*, Shanghai, China, Oct. 30–Nov. 02, 2008, Paper SaN3, .